Domain evidence for canted noncollinear interlayer coupling

Shi-shen Yan*
Center for Materials for Information Technology, The University of Alabama, Tuscaloosa, Alabama 35487-0209

P. Grünberg
Institut für Festkörperforschung, Forschungszentrum Jülich GmbH, D-52425 Jülich, Germany

R. Schäfer
IFW, Helmholtzstraße 20, D-01069 Dresden, Germany
(Received 11 April 2000)

Domain observation by Kerr microscopy was carried out on Fe/Mn/Fe wedge-shaped sandwiches, which were prepared by molecular-beam epitaxy under optimal conditions. For the single-crystal (001)-oriented Fe layers with fourfold in-plane anisotropy, besides the four kinds of well-known domain patterns of ferromagnetic coupling, antiferromagnetic coupling, 90° coupling, and no coupling, we found a fifth kind of domain pattern. The interpretation of these domains inevitably results in the finding of the trivial canted noncollinear coupling between two Fe layers. The magnetic phase diagram of the coupling was analyzed according to the proximity magnetism model. We also found that the domain characters, the coercive field, and the coupling angle are closely related to one another. This investigation indicates that domain observation is a useful and sensitive method to detect locally the coupling types in the wedge-shaped sandwiches.

I. INTRODUCTION

Interlayer coupling between two magnetic layers through a spacer layer, for instance, Fe/Cr/Fe trilayers,[1] is often found to oscillate periodically from ferromagnetic (FM) to antiferromagnetic (AF) as the thickness of the spacer layer varies, and there exist transitional zones of 90° coupling between FM and AF coupling. For (001)-oriented single-crystal Fe layers with fourfold in-plane anisotropy, the magnetization vectors in the same area of two Fe layers are respectively parallel, antiparallel, and perpendicular to each other in the cases of FM, AF, and 90° coupling, but they still remain in the four directions of the two easy axes, which makes it easy to analyze the coupling type by directly observing domain structure.[1–3] However, the direct domain evidence for trivial canted noncollinear states is still missing though the canted coupling has been found in a few cases,[4–7] such as 50° coupling in Fe/Cr multilayers,[4] 135° coupling in FeNi/Ag multilayers,[5] canted coupling in Fe/Cr/Fe trilayers,[6] and canted coupling in Fe/Mn/Fe trilayer.[7] In Fe/Cr/Fe trilayers[6] only the magnetization vector of the top Fe layer could be detected by the SEMPA method, so it was impossible to know the exact coupling angle between the magnetization vectors of the top Fe layer and the bottom Fe substrate. By contrast, in the wedge-shaped Fe/Mn/Fe trilayer[7] the canted coupling angle between the magnetization vectors of the two Fe layers in the remanent state was obtained by fitting the theoretical calculation to the experimental hysteresis loops measured by magneto-optical Kerr effect (MOKE). The coupling angle increases gradually from 0° to about 180° and then reduces to 90° when the thickness of Mn layer varies from 0.62 to 1.2 nm. For Mn layer thicknesses in the range between 1.2 and 2.45 nm, the interlayer coupling is always of the 90° type, but its strength oscillates with a short period of two monolayers of Mn. In this paper domain observation was carried out on the same Fe/Mn/Fe trilayer and direct domain evidence for canted interlayer coupling is given.

II. EXPERIMENT

The Fe(5 nm)/Mn(0–4 nm)/Fe(5 nm) wedge-shaped sandwich was epitaxially deposited in UHV by thermal evaporation onto a GaAs/Fe(1 nm)/Ag(150 nm) substrate-buffer system of 6×16 mm dimensions as described elsewhere.[7] The sample plane is parallel to the (001) crystallographic plane, and the single-crystal Fe layers show fourfold in-plane anisotropy with easy directions along the $\langle100\rangle$ axes. The long dimension of the sample is along the [100] easy axis of Fe, which is the gradient direction of the Mn layer thickness, and the wide dimension of the sample is along the [010] easy axis. The whole sample was covered and protected by a ZnS antireflection coating which enhances at the same time the magneto-optical effect.

The domains were observed by magneto-optical Kerr microscopy using a digital contrast enhancement scheme.[8] The yellow spectrum line of a mercury arc lamp was employed. Due to the opaque GaAs substrate, only the top side of the sample could be investigated. In our sample the thickness of each Fe layer is 5 nm, which is less than the penetration depth (about 20 nm) of light in iron layer. Thus the magneto-optical contrast is mainly determined by the top Fe layer, but the bottom Fe layer has also significant contributions to the contrast. During domain observation, an in-plane magnetic field could be applied along all directions. The domain pictures, without specific statement, were taken at remanent states.

III. RESULTS AND DISCUSSION

We first show in Fig. 1 some characteristic domain patterns observed on the whole Fe/Mn/Fe wedge-shaped trilayer. Figures 1(a) and (b) show typical domains of the

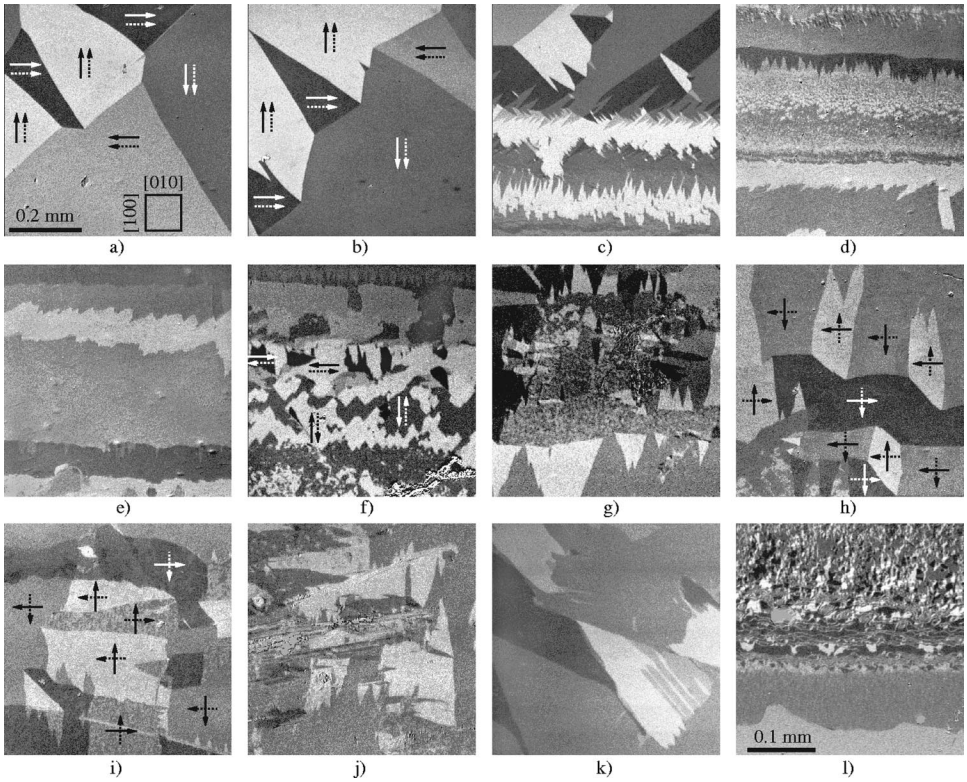

FIG. 1. Some characteristic domain patterns observed along the whole length of the Fe/Mn/Fe wedge-shaped trilayer. The Mn layer thickness varies in the [100] direction (the Mn thickness increases from top to bottom in each image), and its thickness range is, respectively, (a) 0.08–0.25 nm, (b) 0.25–0.42 nm, (c) 0.38–0.55 nm, (d) 0.5–0.67 nm, (e) 0.62–0.79 nm, (f) 0.79–0.96 nm, (g) 1.0–1.17 nm, (h) 1.13–1.3 nm, (i) 1.25–1.42 nm, (j) 1.5–1.7 nm, (k) 2.5–2.7 nm, and (l) 0.55–0.63 nm. The solid arrows indicate the magnetization direction of the top Fe layer and the dotted arrows indicate the magnetization direction of the bottom Fe layer. From (a) to (k) the domain pictures have the same scale as shown in (a). (l) is a higher resolution domain image.

area of FM coupling: The domains are relatively wide and regular in shape, and at most show four gray contrasts according to the four available easy directions for magnetization vectors; the domain walls are 90° walls and 180° walls, and they can be moved easily by a small field (coercive field about 4 Oe). According to the principle of flux closure and stray field avoidance, the regular domain patterns are expected in the area of FM coupling.

The middle part of Fig. 1(f) shows typical domain features of AF coupling: The domains still show four gray contrasts, but they are quite irregular and different in shape and size; the domain walls can be oriented to arbitrary directions, and a relatively high field is needed to move these walls as compared with the coercive field in the FM area. If both Fe layers are coupled antiferromagnetically at very point of this area, their magnetization flux will cancel locally. In this case any orientation of a domain wall is possible and the actual formation of domain walls will be determined by random influences.

The third kind of well-known domain patterns is shown in Figs. 1(h)–1(j). These domains are typical for 90° coupling: Most regular domain walls are aligned along easy directions or are oriented at 45° to the easy directions, but there are also a few peculiar rugged walls; the domains show eight gray contrasts (at most) and the coercive field is small. The eight gray contrasts are caused by eight possible configurations of the magnetization vectors in the two Fe layers. In every configuration, the magnetization vectors at the same point of the two Fe layers align along different easy directions and perpendicular to each other, so the net magnetization is in hard axis directions. According to the same principle of flux closure and stray field avoidance, rugged walls are formed between domains with the same net magnetization but different magnetization configurations coming from interchanging the magnetization directions of the two Fe layers. On the other hand, regular domain walls are formed when the direction of the net magnetization does change. So there is no doubt that the interlayer coupling in Figs. 1(h)–1(j) is of the 90° type.

The fourth kind of domain is shown in Fig. 1(k). They are typical domains in the area of very weak coupling or without coupling. At first glance the domains are similar to those of FM coupling and the domain walls can be moved easily by a small field. However, the domain walls are not as straight and regular as those of FM coupling, and domains show many gray contrasts (at most 16 possible gray contrasts for our sample). In this case the Mn interlayer is so thick that there is no coupling or the coupling strength is less than the coercive field. As a result the magnetization configurations in the two Fe layers are mainly determined by the coercive field and the two magnetization vectors are not related to each other. So the domains with the above features can be observed in this area. In the following paragraphs we mainly pay our attention to the area of strong interlayer coupling, where domain features are mainly determined by the coupling type (coupling angle).

Except the well-known four kinds of domain patterns ex-

plained before, there exists a fifth kind of domain patterns as shown in the bottom part of Fig. 1(c), and in Figs. 1(d) and 1(e), which are quite different from all other domain patterns in the trilayers with coupling.[1–3] The whole domain images are composed of stripelike structures, and the edges of the stripes are perpendicular to the gradient direction of the Mn layer. Near the area of FM coupling, dense zigzag domain walls are found at the edges of the stripelike structures, as shown in the bottom part of Fig. 1(c). With increasing the thickness of Mn layer, the zigzag domain walls gradually develop into less rugged domain walls, as shown from Figs. 1(c)–1(e). Moreover, these stripes show many gray contrasts, and even one stripe is sometimes not a single domain, but composed of a lot of small patchlike domains, as shown in Figs. 1(d) and 1(l).

Another surprising feature of these stripelike domains is that with a gradual increase of the external field (in arbitrary given direction) the edges (or domain walls) of the stripelike domains can be shifted smoothly in the gradient direction of the Mn thickness until near the area of AF coupling. But if the external field stops increasing and then is reduced to zero, the shift of the domain walls will stop and the domains will almost stay unchanged during this process. This phenomenon can be explained essentially by the assumption that when the Mn layer thickness varies the coupling angle in the remanent state varies and as a result the coercive field varies. We will discuss this in detail in the following paragraphs. In fact, we can easily get the domain images of Figs. 1(c)–(e) in the following way: Assuming $H_1>H_2>H_3\cdots>H_n=0$ (the external field is along the [010] easy axis), when we reduce the external field from saturation to zero and then reverse it and increase its strength to $-H_1$, a stripe domain wall (the first one) can be generated near the FM area and then shifts close to the AF area. If we consequently change the external field from $-H_1$ to zero, and then reverse it and increase its strength to H_2, the second stripe domain wall can be generated near the FM area and then shifts towards the first one. Owing to $H_2<H_1$, the first domain wall almost does not change during the shift of the second domain wall. Repeating the above process, we can get a lot of stripelike domains and the whole domain pictures are finally taken at zero magnetic field. By the way, the stripelike domain patterns are highly reproducible. However, the stripelike domains cannot be observed in any area of pure coupling type, such as FM, 90° and AF, even if in this area the thickness of Mn layer varies and the strength of the pure coupling is different. Therefore we think the fifth area is composed of different canted states and the coupling angles of these states can gradually vary with increasing the thickness of Mn layer.

Figure 2 shows the domain patterns of the FM area and its neighbor area after alternating current (ac) demagnetization. The ac field is parallel to the [010] easy axis. It is clear that the whole FM area becomes a single domain state after ac demagnetization, as shown in the top part of the domain patterns. However, the neighbor area shows quite different domain structures, as shown in the bottom part of the domain patterns. We can see obvious ripplelike domain structures though the gray contrast is not strong. If we subsequently apply a small field to the above domains, rotate the field gradually and then reduce the field to zero, Fig. 2 develops into Fig. 3. The single domain state in FM area develops into

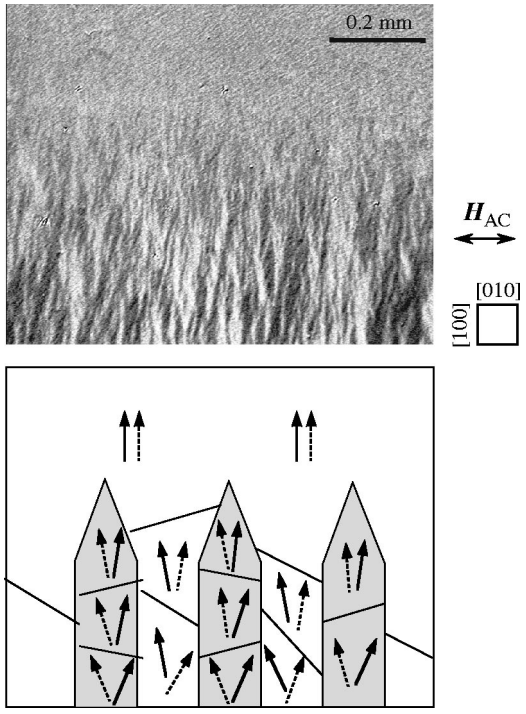

FIG. 2. Domain patterns in the area of FM coupling and its neighbor area after alternating current demagnetization. The bottom part is a schematic diagram of the single domain state in the FM area and the ripplelike domains in its neighbor area. The solid arrows indicate the magnetization direction of the top Fe layer and the dotted arrows indicate the magnetization direction of the bottom Fe layer.

domains with four gray contrasts. The ripplelike domains also become domains with four main gray contrasts. But for each main gray contrast, we can still see two subcontrasts from the remaining ripplelike structures. So the ripplelike domains can develop into eight gray contrasts at most. In order to explain the above phenomenon, we must assume that the neighbor area of FM has a canted interlayer coupling and the canted coupling angle is very small. As a result, the canted coupling state only shows small deviation from the FM coupling state. If the magnetization vectors in the two Fe layers deviate symmetrically from the easy directions by small angles $\pm\theta/2$ (the coupling angle is θ), the net magnetization is still in four easy directions. So we can see four main gray contrasts. But for the same net magnetization, we can get two magnetization configurations by interchanging the magnetization vectors of two Fe layers. Because the coupling angle is very small, the gray subcontrasts coming from these two configurations are very weak. For the same reason, the very weak gray contrast of ripplelike domains in Fig. 2 can be explained by the two magnetization configurations with the same net magnetization.

IV. THEORETICAL ANALYSIS AND DISCUSSION

To give an overview on the coupling of Fe/Mn/Fe trilayers, we calculate the phase diagram of the coupling. For the description of exchange coupling across antiferromagnetic interlayer materials (such as Mn and Cr) with thickness fluctuations due to interface roughness, the proximity magnetism model of Slonczewski[9] should be used. In this phenomeno-

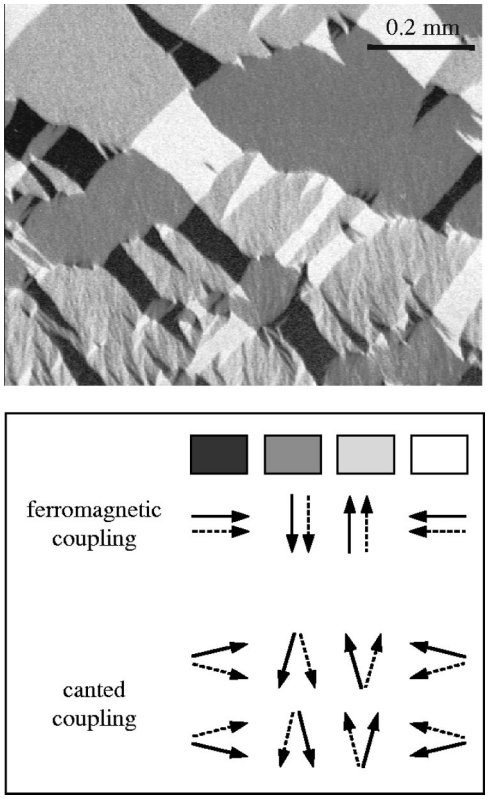

FIG. 3. Domain patterns evolving from the domains in Fig. 2. The bottom part is a schematic explanation of the observed domains. By carefully comparing the four gray contrasts in the FM area with those in its neighbor area, we can come to the conclusion that the canted coupling with small coupling angle has four main gray contrasts and each main gray contrast includes two subcontrasts.

logical model, the exchange coupling energy per unit area can be written as

$$E_C = C_+(\theta)^2 + C_-(\theta-\pi)^2, \tag{1}$$

where $C_+ \geqslant 0$, $C_- \geqslant 0$, and $0 \leqslant \theta \leqslant \pi$. Here C_+ and C_- are two coupling coefficients to describe the strength of the interlayer coupling, and θ is the angle between the magnetization vectors in the two Fe layers. Taking into account the cubic anisotropy energy of the Fe layers, Zeeman energy in external field, and interlayer coupling in the form of Eq. (1), the magnetic phase diagram can be obtained by minimizing the total energy of Eq. (3) in Ref. 7 with respect to ϕ_1 and ϕ_2 at a given external field H for the appropriate C_+ and C_-. Here ϕ_1 (ϕ_2) is the angle between the magnetization vector of the first (second) Fe layer and the easy direction. Figure 4 shows the phase diagram of the coupling at zero field. The interlayer coupling is of the FM type only in the case of $C_+ > 0$ and $C_- = 0$, and is of the AF type only in the case of $C_- > 0$ and $C_+ = 0$. The 90° coupling can occur only when $C_+ = C_- > 0$. In the above three types of coupling, the two magnetization vectors are always aligned in the easy directions at zero field. In all other cases of coupling, the coupling is trivial canted noncollinear coupling, in which the two magnetization vectors will deviate from the easy directions. For the region of $C_- - 3C_+ > 0$, the two magnetization vectors deviate symmetrically from the easy directions and the coupling angle is in the range of $3\pi/4 < \theta \leqslant \pi$. For the

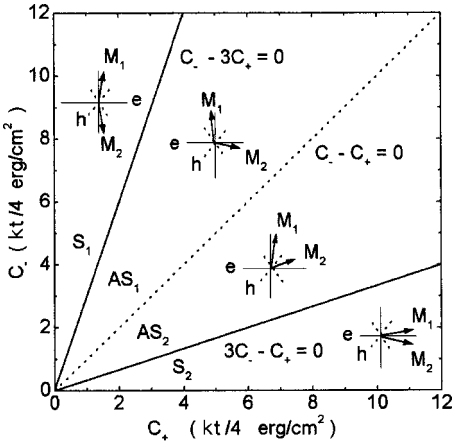

FIG. 4. Magnetic phase diagram of the interlayer coupling at zero field. S indicates that the two magnetization vectors are symmetrical about the easy axis (e), and AS indicates that the two magnetization vectors are asymmetrical about the easy axis but symmetrical about the hard axis (h). The boundaries (solid lines) between the two phases (S and AS) are two straight lines, i.e., $C_- - 3C_+ = 0$ and $3C_- - C_+ = 0$. The dotted line is $C_- - C_+ = 0$. The inserted symbols show schematically the nonequal magnetization configurations in the two Fe layers. For the same canted angle, there are eight equal magnetization configurations with the same energy at zero field. $K = 4.76 \times 10^5$ erg/cm^3 is the first-order in-plane anisotropy of (001) Fe layer, and $t = 5 \times 10^{-7}$ cm is the thickness of each Fe layer (the thickness of two Fe layers is equal).

region of $3C_- - C_+ < 0$, the two magnetization vectors deviate also symmetrically from the easy directions and the coupling angle is in the range of $0 \leqslant \theta < \pi/4$. But for the region of $C_- - 3C_+ < 0$ and $3C_- - C_+ > 0$, the two magnetization vectors deviate symmetrically from the hard directions and the coupling angle is in the range of $\pi/4 < \theta < 3\pi/4$.

Figure 5 shows the experimental results of the coupling coefficients C_+ and C_-, the coupling angle θ in the remanent state, and the coercive field H_C of the Fe/Mn/Fe trilayer. The coercive field was directly obtained from the hysteresis loops measured by MOKE. The coupling coefficients and the coupling angle in the remanent state were obtained by fitting the theoretical calculation to the experimental hysteresis loops using Eq. (3) in Ref. 7. Although the coupling angle in the remanent state is only determined by the coupling coefficients C_+ and C_- (anisotropy K and saturation magnetization M are constants for Fe layers) through Eq. (3) in Ref. 7, the dependence of the coupling angle on the thickness of the Mn layer [see Fig. 5(b)] is quite different from that of the coupling coefficients [see Fig. 5(a)]. But the dependence of the coupling angle on the thickness of Mn layer [see Fig. 5(b)] is similar to that of the coercive field [see Fig. 5(c)]. In fact, the magnetization vectors are strongly coupled for thin Mn layer in the Fe/Mn/Fe trilayer, and the magnetization reverses by displacement of domain walls which can be seen by domain observation. For the strong coupling case, we can assume that the coupling angle almost does not change when the applied field varies from the remanent state to the coercive field. We can further assume that all the domain walls are pinned by the same pinning energy ε and magnetization reversal is caused by the displacement of 180° domain walls. According to the phase diagram in Fig. 4, when the two magnetization vectors in the remanent state deviate sym-

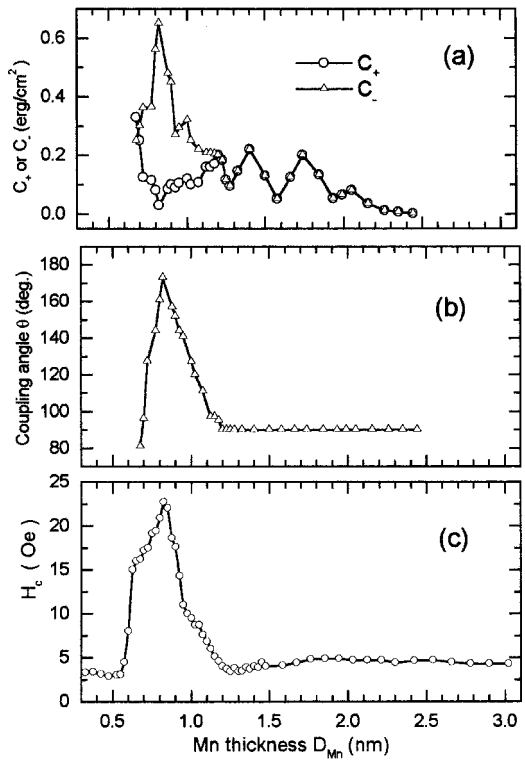

FIG. 5. The Mn layer thickness dependences of (a) the coupling coefficients C_+ and C_- (Ref. 7), (b) the coupling angle θ in remanent state (Ref. 7), and (c) the coercive field H_c of the Fe/Mn/Fe trilayer.

metrically from the easy direction by the angles $\pm\theta/2$ (θ is the coupling angle) and the applied field is parallel to the same easy axis, the coercive field can be given as the following:

$$2H_C M\cos(\theta/2)=\varepsilon,$$

$$H_C=\varepsilon/[2M\cos(\theta/2)]=H_{\mathrm{FC}}/\cos(\theta/2), \qquad (2)$$

where $H_{\mathrm{FC}}=\varepsilon/(2M)$ is the coercive field in the area of FM coupling, and $0\leqslant\theta<\pi/4$ or $3\pi/4<\theta\leqslant\pi$.

When the applied field is still parallel to the same easy axis but the two magnetization vectors deviate symmetrically from the hard axis by the angles $\pm\theta/2$, we can get

$$2H_C M\cos(\theta/2)\cos(\pi/4)=\varepsilon,$$

$$H_C=\varepsilon/[2M\cos(\theta/2)\cos(\pi/4)]=\sqrt{2}H_{\mathrm{FC}}/\cos(\theta/2), \quad (3)$$

where $\pi/4<\theta<3\pi/4$. Our simple model calculation indicates that the coercive field is proportional to the reciprocal of $\cos(\theta/2)$, so the coercive field increases (or reduces) as the coupling angle increases (or reduces) in the range of $0\leqslant\theta\leqslant\pi$, which is qualitatively in agreement with the experimental results in Figs. 5(b) and 5(c). This is why we can observe the stripelike domains in the area of canted coupling states.

From the above analysis, it is easy to explain the domain characters of the trivial canted coupling states as shown in Figs. 1(c)–1(e). With increasing the thickness of the Mn layer from FM coupling to AF coupling, the canted coupling angle gradually increases from 0° (FM coupling) to about 180° (AF coupling) and as a result the coercive field gradually increases. So we can observe stripelike domain structures in the trivial canted coupling area and the domain walls can be shifted smoothly with the increase of the external field. Even for the same canted coupling angle, there exist eight possible magnetization configurations. So when the coupling angle gradually changes in the canted coupling area, we can see many gray contrasts of the Kerr effect. On the other hand, the local net magnetization at zero field will become small when the coupling angle gradually becomes big. So the zigzag domain walls which are full of the edges of the stripelike domain structures near FM coupling area will gradually develop into less rugged domain walls of the stripelike domains near the AF coupling area.

Finally, we will compare the domain observation with the measurements of hysteresis loops. From the viewpoint of experimental measurements, the hysteresis loops are sensitive to the coupling strength and the coupling angle difference between the remanent state and saturation state, but domain patterns are sensitive to the coupling angles at the remanent states. So in the cases of FM coupling, or the canted coupling with very small coupling angle, or very weak coupling (including no coupling) less than the coercive field, it is almost impossible to distinguish them from the shape of the hysteresis loops, but the domain structures are quite different for the above cases, as shown in Figs. 1(a)–1(c), 1(k), 2, and 3. On the other hand, the hysteresis loops measured by MOKE indicate that when the Mn thickness increases from 1.2 to 2.45 nm the coupling is always of the 90° type and its strength oscillates with a short period of 2-Mn monolayers (about 0.365 nm), as shown in Figs. 5(b) and (a). However, the domain characters [see Figs. 1(h)–1(j)] are the same in this case because the coupling angle at the remanent state is the same. So domain observation and hysteresis loop measurements can be mutually complementary in the study of the interlayer coupling, and especially domain observation is appropriate to study the coupling type for the wedge-shaped samples.

V. CONCLUSIONS

In conclusion, magnetic domains were observed on the Fe/Mn/Fe wedge-shaped sandwiches by Kerr microscopy. Besides the four kinds of well-known domain patterns of ferromagnetic coupling, antiferromagnetic coupling, 90° coupling and no coupling, we found a fifth kind of domain patterns. The interpretation of these domains inevitably results in the findings of the trivial canted noncollinear coupling between two Fe layers. The magnetic phase diagram of the coupling was analyzed according to the proximity magnetism model. This investigation indicates that domain observation is a useful and sensitive method to detect locally the coupling types in the wedge-shaped sandwiches.

*Corresponding author. FAX: 205-3482346. Email address: syan@mint.ua.edu

[1] M. Rührig, R. Schäfer, A. Hubert, R. Mosler, J. A. Wolf, S. Demokritov, and P. Grünberg, Phys. Status Solidi A **125**, 635 (1991).

[2] Jeffery McCord, Alex Hubert, Rudolf Schäfer, Achim Fuss, and Peter Grünberg, IEEE Trans. Magn. **29**, 2735 (1993).

[3] Rudolf Schäfer, J. Magn. Magn. Mater. **148**, 226 (1995).

[4] A. Schreyer, J. F. Ankner, Th. Zeidler, H. Zabel, M. Schäfer, J. A. Wolf, P. Grünberg, and C. F. Majkrzak, Phys. Rev. B **52**, 16 066 (1995).
[5] Bernard Rodmacq, Karine Dumesnil, Philippe Mangin, and Martine Hennion, Phys. Rev. B **48**, 3556 (1993).
[6] D. T. Pierce, J. Unguris, R. J. Celotta, and M. D. Stiles, J. Magn. Magn. Mater. **200**, 290 (1999).
[7] Shi-shen Yan, R. Schreiber, F. Voges, C. Osthöver, and P. Grünberg, Phys. Rev. B **59**, R11 641 (1999).
[8] F. Schmidt, W. Rave, and A. Hubert, IEEE Trans. Magn. **21**, 1596 (1985).
[9] J. C. Slonczewski, J. Magn. Magn. Mater. **150**, 13 (1995).